Inelastic neutron scattering investigation of magnetostructural excitations in the spin-Peierls organic system $(TMTTF)_2PF_6$

J. P. Pouget,[1] P. Foury-Leylekian,[1] S. Petit,[2] B. Hennion,[2] C. Coulon,[3] and C. Bourbonnais[4]

[1]*Laboratoire de Physique des Solides, Centre National de la Recherche Scientifique (CNRS) UMR 8502, Bâtiment 510, Université Paris Sud, 91405 Orsay Cedex, France*

[2]*Laboratoire Léon Brillouin, Centre d'Etudes Atomiques (CEA), CNRS, Université Paris-Saclay, CE-Saclay F-91191 Gif sur Yvette Cedex, France*

[3]*CNRS and Université de Bordeaux, Centre de Recherche Paul Pascal, UPR 8641, F-33600 Pessac, France*

[4]*Regroupement Québécois sur les Matériaux de Pointe, Département de Physique, Université de Sherbrooke, Sherbrooke, Québec, Canada, J1K-2R1*

(Received 9 May 2017; revised manuscript received 20 June 2017; published 17 July 2017)

One-dimensional (1D) conductors such as Bechgaard and Fabre salts are a prototypal example of correlated systems where the phase diagram is controlled by sizable electron-electron repulsions. In deuterated $(TMTTF)_2PF_6$, where this interaction achieves charge localization at ambient pressure on donor stacks, magnetostructural coupling plays a decisive role to stabilize a spin-Peierls (SPs) ground state at $T_{SP} = 13$ K. In this paper, we present the first inelastic neutron scattering investigation of SP magnetic excitations in organics. Our paper reveals the presence above T_{SP} of sizable critical fluctuations leading to the formation of a pseudogap in the 1D antiferromagnetic (AF) $S = 1/2$ magnetic excitation spectrum of the donor stack, concomitant with the local formation of singlet of paired spins into dimers below $T_{SP}^{MF} \approx 40$ K. In addition, the inelastic neutron scattering investigation allows us also to probe the SP critical lattice dynamics and to show that at ambient pressure these dynamics are of relaxation or order-disorder type. Below T_{SP}, our paper reveals the emergence of a two gap SP magnetic excitation spectrum towards a well-defined $S = 1$ magnon mode and a continuum of two excitations, as theoretically predicted. Our measurements allow us to locate the ambient pressure SP phase of $(TMTTF)_2PF_6$ in the classical (adiabatic) limit close to the classical/quantum crossover line. Then we provide arguments suggesting that pressurized $(TMTTF)_2PF_6$ shifts to the quantum (antiadiabatic) SP gapped phase, which ends in a quantum critical point allowing the stabilization of an AF phase that competes with superconductivity at higher pressure. Finally, we propose that the magnetostructural coupling mechanism in the Fabre salts is caused by dimer charge/spin fluctuations driven by the coupling of donors with anions.

DOI: 10.1103/PhysRevB.96.035127

I. INTRODUCTION

There is a general consensus that a reduction of spatial dimension in systems of interacting electrons magnifies quantum effects and enhances instabilities towards collective states of matter [1]. This is a consequence of interactions between electrons, which in reduced dimensions behave in a highly organized and collective manner. These considerations are well illustrated in several classes of low dimensional metals such as copper oxide superconductors [2], transition-metal dichalcogenides [3], and organic conductors [4] whose complex phase diagram is still the subject of intensive debates. In these different systems, it is found in particular that superconductivity emerges in close proximity to other collective states where magnetic or charge degrees of freedom order into either spin- or charge-density wave (SDW or CDW) structures. Among these materials, a special attention has been devoted to one-dimensional (1D) organic conductors such as the first organic superconductors $(TMTSF)_2X$, the Bechgaard salts, and the charge/Mott localized $(TMTTF)_2X$ Fabre salts [4]. TMTSF stands for tetramethyl-tetraselenafulvalene, TMTTF for tetramethyl-tetrathiafulvalene, and X for a monovalent anion.

The isostructural Bechgaard and Fabre salts present a generic phase diagram controlled by quantum effects [5]. On the $(TMTTF)_2X$ side, Mott localization of one hole per TMTTF dimer occurs around 240 K (T_ρ), in which the energy scale is much smaller than the electron bandwidth ($\sim$0.8 eV), indicating that the electrons are weakly localized over relatively large distances by the Coulomb repulsion. The Mott localization is followed by a charge ordering (CO)/ferroelectric transition at 87 K in the deuterated PF_6 salt studied here. These two features achieve a spin-charge decoupling. At lower temperature, the remaining $S = 1/2$ degrees of freedom (one spin per dimer) either couple in an antiferromagnetic (AF) manner, at $T_{AF} = 8$ K for $X = SbF_6$, or pair into a spin-Peierls (SPs) singlet state, at $T_{SP} = 16.5$ K and 11 K for hydrogenated $X = PF_6$ and AsF_6 salts, respectively. The Mott scale T_ρ progressively decreases under pressure, while the CO transition is quickly suppressed, and the SP ground state transforms into an AF one via a quantum critical point (QCP) around $P_{QCP} \approx 0.9$ GPa for $X = PF_6$ [6]. At higher pressure when T_ρ vanishes, the AF ground state changes into a $2k_F$ SDW ground state as found in metallic $(TMTSF)_2PF_6$ at ambient pressure (k_F is the Fermi wave vector of the quasi-1D metal). Under additional pressure, an anomalous metallic phase develops in an extended low temperature quantum critical domain connecting the optimal ordering temperature for superconductivity ($T_S \sim 1$ K) to the vanishing of the SDW phase [7].

As organics are soft materials [8], the coupling of electronic degrees of freedom to the lattice in the Bechgaard and Fabre salts should be considered for a realistic description of the phase diagram. Indeed, the CO ground state of Fabre salts is

accompanied by noticeable lattice deformations [9,10], and SP singlets are stabilized by a dimerization of the stack of TMTTF dimers, which transversally couple at T_{SP} by forming a three-dimensional (3D) (1/2, 1/2, 1/2) superstructure [11]. Interestingly, the SP instability is due to a sizeable magnetoelastic coupling that manifests itself in a large regime of 1D pretransitional fluctuations at $q_{SP} = a^*/2$ starting well above T_{SP}, up to 60 K and 40 K (identified below as the mean-field SP temperature T_{SP}^{MF}) for hydrogenated $X = PF_6$ and AsF_6 salts, respectively [12]. Also the q_{AF} AF order of $(TMTTF)_2Br$ is accompanied by a $2q_{AF}$ magnetoelastic lattice deformation, and, more surprisingly, the SDW ground state of $(TMTSF)_2PF_6$ stabilizes a $2k_F$ SDW-CDW hybrid modulation [13,14]. Finally it has been recently pointed out that the electron-phonon interaction could have a significant influence in a SDW driven mechanism of superconductivity [15].

The SP ground state opens a gap in the excitation continuum of the Heisenberg and XY $S = 1/2$ AF chains by picking out the singlet components of AF quantum fluctuations [1]. In this ground state, the singlet configurations are stabilized by the pairing of neighboring $S = 1/2$ spins into dimers via a structural instability achieved by magnetoelastic coupling between spin and lattice degrees of freedom. The 0 K phase diagram of the SP chain, calculated in Refs. [16] and [17] for the XY and Heisenberg $S = 1/2$ AF chains respectively, is quite subtle:

(1) Depending on the relative value of the SP gap Δ (or more likely of its mean-field value, Δ^{MF}) with respect to the q_{SP} critical phonon energy $\hbar\Omega_C$, the SP ground state is either of classical nature (for large Δ^{MF}) or of quantum nature (for small Δ^{MF}).

(2) For a weak SP gap, the zero point phonon quantum fluctuations kills the lattice dimerization, and the quantum SP gap vanishes exponentially at a QCP beyond which a spin liquid state is stabilized.

For the Heisenberg chain, the crossover from a gapped classical (adiabatic) SP ground state to a quantum (antiadiabatic) SP ground state occurs for $\hbar\Omega_C \approx \Delta^{MF}/2$ [17], and the quantum SP ground state vanishes when $\Delta^{MF} \sim 0.7\hbar\Omega_C$ [18] $-0.4\hbar\Omega_C$ [17].

Estimation of microscopic parameters shows that organic SP compounds are located either in the classical region, as in $(BCP-TTF)_2X$, or in the quantum region, as in MEM-$(TCNQ)_2$, while the Fabre salts should be located in the vicinity of the classical-quantum crossover [19] (see also Fig. 10 in Ref. [20]); BCP-TTF is benzo-cyclopentyl-tetrathiafulvalene, MEM is methyl-ethyl-morpholinium, and TCNQ is tetracyano-quinodimethane. The inorganic SP compound $CuGeO_3$ is also located in the quantum region but in the vicinity of the QCP line at which the SP ground state vanishes.

In the adiabatic limit, the conjoint treatment of AF quantum $S = 1/2$ spins and structural SP fluctuations show the development of a pseudogap in the spin susceptibility when the 1D SP fluctuations start to develop below the mean field temperature T_{SP}^{MF}, in agreement with experimental findings in $(BCP-TTF)_2X$ [21] (for the Heisenberg chain, T_{SP}^{MF} is related to Δ^{MF} by the mean-field correspondence relationship $\Delta^{MF} \approx 2.47\, k_B T_{SP}^{MF}$ [22]). However, until now there is no direct measurement of the influence of magnetostructural SP fluctuations on the AF spin excitation spectrum above T_{SP} and of the excitation spectrum in the SP ground state in organics. In this paper, we report the first inelastic neutron scattering investigation of such effects in deuterated $(TMTTF)_2PF_6$.

II. EXPERIMENTALS

A. Neutron scattering conditions

In order to reduce the important background due to incoherent neutron scattering on proton, the inelastic neutron scattering investigation has been performed with 97.5% deuterated $(TMTTF)_2PF_6$ (PF_6-D12 below), prepared according to Ref. [23]. In order to increase the signal-to-noise ratio to detect singularities in the magnetic excitation spectrum, 1 cm^3 of powder was obtained by crushing several PF_6-D12 crystals. A previous study reported in Ref. [24] proved the possibility of detection of a quasi-1D magnetic neutron scattering response from a PF_6-D12 powder. Here we report a complete study of the magnetic fluctuations associated to the SP instability above T_{SP} (run 1) and of the SP excitations below T_{SP} (run 2) using the triple axis spectrometer 2T installed at the Orphée reactor (Laboratoire Léon Brillouin, Saclay, France). Energy scans were recorded below 20 meV in the creation mode of excitation, with fixed $k_F = 2.662$ Å^{-1} and $Q = 1.66$ Å^{-1}. The Q corresponds to the position $Q_{SP} = (3/2, -\frac{1}{2}, \frac{1}{2})$ of one of the most intense SP superlattice reflections observed in previous neutron scattering investigations [11,25]. To increase the statistics, each scan has been measured several (between 2 and 12) times and then averaged. For run 1, the global counting time was of ~1 h per point. In order to achieve better statistics, the counting time was 3.5 times longer in run 2. This paper has been completed by the measurement of low energy phonon modes at Q_{SP} in a large PF_6-D12 single crystal taken from the same batch (see Appendix A).

B. Magnetic characteristics of $(TMTTF)_2PF_6$-D_{12}

The PF_6-D12 has been characterized by its spin susceptibility, χ_S, measured on a single crystal of the same batch. χ_S corrected at constant volume [26] (Fig. 1) exhibits above 20 K both an absolute value and a thermal dependence compatible with a $S = 1/2$ AF Heisenberg chain with a first neighbor exchange interaction $J \approx 39$ meV [27]. This value agrees with $J \sim 35$ meV deduced from the measurement [24] of one minima J_{eff} of the continuum of magnetic excitations in the SP ground state of PF_6-D12 [see Fig. 2(b)]. Above 20 K, χ_S of PF_6-D12 is identical to χ_S of protonated AsF_6-H12 and PF_6-H12 salts [25]. The J values obtained in our investigations are close to exchange interactions previously reported in the literature [28].

Figure 3(a) shows that χ_S exhibits a well-pronounced S-shaped thermal decrease around T_{SP} without exhibiting a clear kink at T_{SP}. The T_{SP} is more clearly defined from the onset temperature, 13 ± 0.1 K, of SP superlattice reflections measured in a single crystal of the same batch [25] and from the temperature, 13.1 K and 13 K, at which, respectively, the microwave dielectric response [23] and the sound velocity [29] exhibit critical singularities. These T_{SP} values coincide also with the maxima at 13.1 K of the derivative $d\chi_S/dT$ plotted in the inset of Fig. 1. Also T_{SP} determined by the maxima of $d\chi_S/dT$ in AsF_6-H12 and PF_6 -H12 [25] coincides with the critical SP singularity of uniaxial lattice expansion [8,9]. This

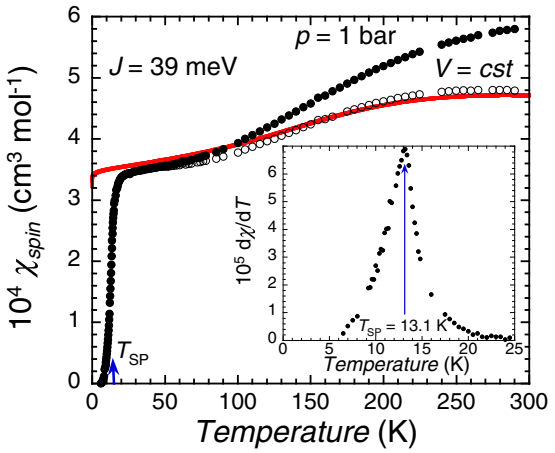

FIG. 1. Temperature dependence of the spin susceptibility, χ_S, of a single crystal of PF_6-D12. The filled circles give the ambient pressure SQUID measurements, and the empty circles give the spin susceptibility at constant volume (the volume correction is performed according to the procedure described in Ref. [26]). The continuous (red) line is the fit of χ_S with the expression of the spin susceptibility of the localized $S = 1/2$ AF Heisenberg chain [27]. The adjustment shown in the figure, and which takes into account of both the absolute value and of the thermal dependence of χ_S, gives $J \approx 39$ meV, which is significantly larger than the energy scale $\Delta_{MF} \sim 9$ meV. The inset plots $d\chi_S/dT$, whose maximum gives $T_{SP} = 13.1$ K.

bunch of measurements leads to consistent T_{SP} values, which differ from T_{SP} values previously reported in the literature from a different analysis of the thermal dependence of χ_S [28].

III. INELASTIC NEUTRON SCATTERING RESULTS

Figure 4 reports the energy dependence of scattered neutron intensity measured at Q_{SP} for selected temperatures between 3 K and 70 K. The raw data reveal, for temperature less than 40 K, a sizeable drop of scattered intensity for energy smaller than about 9 meV.

In an inelastic process, the neutron scattering intensity is proportional to the correlation function $S(\mathbf{q},\omega)$. This quantity, when corrected by the Bose factor $n(\omega)+1$ for creation of excitation, gives the response $I(\mathbf{q},\omega)$ to excitations of the system,

$$S(\mathbf{q},\omega) = [n(\omega)+1]I(\mathbf{q},\omega). \quad (1)$$

In the presence of coherent scattering processes, $I(\mathbf{q},\omega)$ is the sum on all the excitations α,

$$I(\mathbf{q},\omega) = \sum_{\alpha} |F_\alpha(\mathbf{q})|^2 \mathrm{Im}\, D_\alpha(\mathbf{q},\omega). \quad (2)$$

In expression (2), Im $D_\alpha(\mathbf{q},\omega)$ is the imaginary part of the propagator of excitation α, and $F_\alpha(\mathbf{q})$ is the structure factor of the same excitation. Note that in expression (2) one assumes that there is no interference between the various excitations. Powder diffraction performs a $\mathbf{q}$ angular average of expression (2). Here, this average is performed at constant $|\mathbf{q}| = Q = Q_{SP}$. Thus the quantity obtained, which will be named $I(Q_{SP},\omega)$ below, measures the partial density of states at Q_{SP} of all the excitations α.

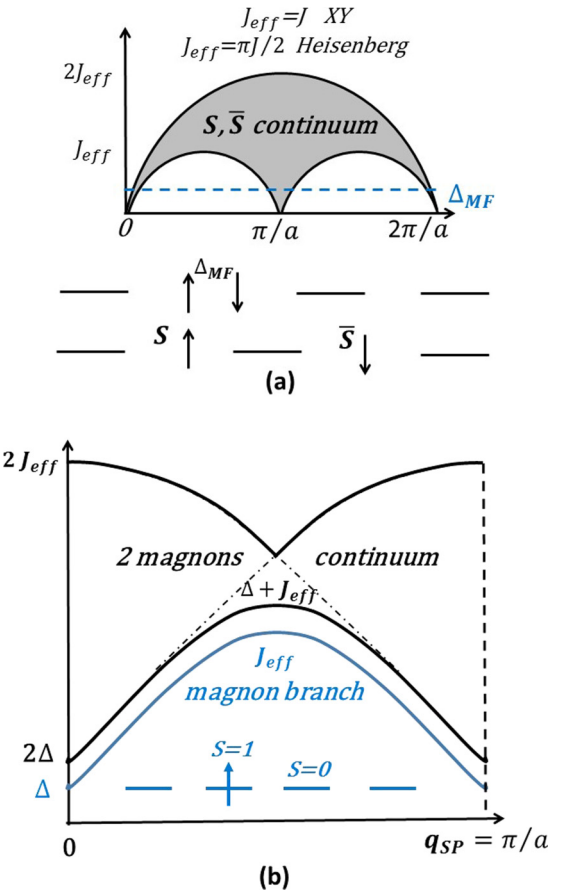

FIG. 2. (a) The 1D spinon excitation spectrum of the Heisenberg/XY $S = 1/2$ AF chain. The energy scale, Δ_{MF}, below which the pseudogap develops, is indicated. The lower part of the figure shows that, in the vicinity of T_{SP}, Δ_{MF} represents the dissociation energy of a dimer into two unpaired spins which, in 1D, can propagate independently under the form of soliton (S) and antisoliton ($\bar{S}$). This free propagation gives rise to the continuum of excitation represented in the upper part of the figure. (b) Quasi-1D magnetic excitation spectrum in the SP ground state according to the RPA theory of Ref. [44]. The magnon mode corresponding to the propagation of a triplet excitation of the dimer, of energy cost Δ, is schematically represented in the bottom part of the figure. The continuum of excitations starting at 2Δ corresponds to the free propagation of two magnons.

Neutron scattering probes both magnetic and phonon excitations of $(TMTTF)_2PF_6$. Magnetic excitations, represented above and below T_{SP} in Figs. 2(a) and 2(b), respectively, are basically of quasi-1D nature. Thus, neutron experiment on powder at Q_{SP} allows us to obtain the density of states at $2k_F^{SDW}$ or q_{SP} of the continuum of magnetic excitations. It allows us to locate extremes of the 1D continuum and of the 1D well-defined dispersions from the detection of maxima of intensity in the diffraction spectrum, as proven by previous numerical simulations of the intensity map [24]. Acoustic phonon modes detected in single crystal measurements at Q_{SP} (see Appendix A) do not contribute to maxima in the phonon density of states. Only nondispersive Einstein-type phonon modes give rise to a peak in the density of states. This is the case of phonon modes giving rise to the temperature independent

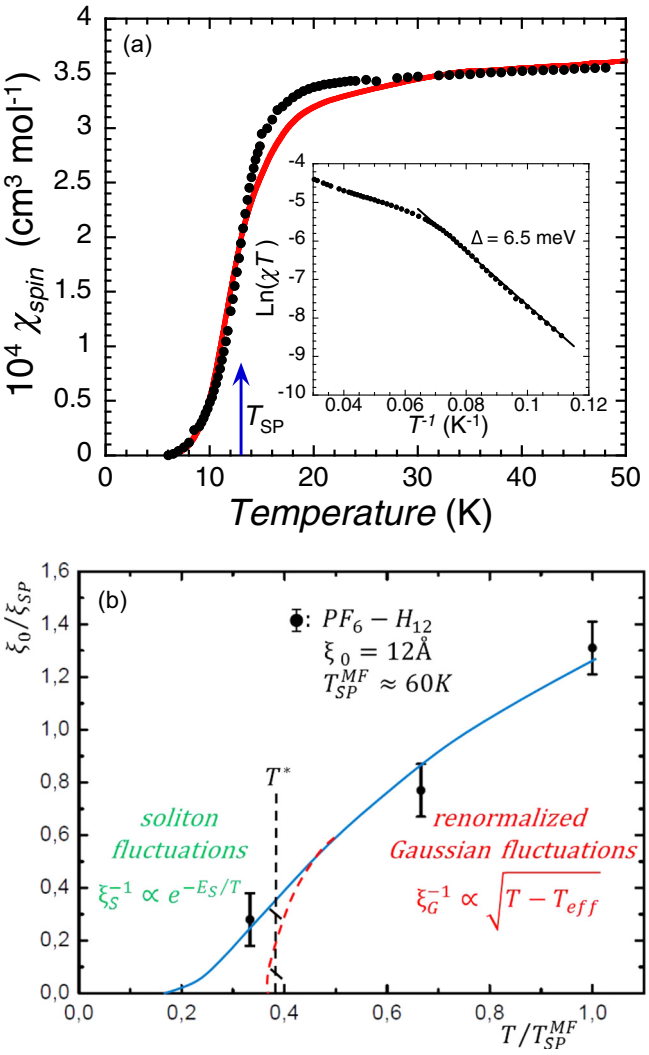

FIG. 3. (a) Thermal dependence of the spin susceptibility, χ_S, of PF_6-D12 in the vicinity of the SP transition. The continuous (red) line is the thermal dependence of χ_S in the presence of 1D SP fluctuations calculated in Ref. [31]. The theoretical curve has been adjusted to $T_{SP}^{MF} = 40$ K. The inset gives $\ln(\chi_S T)$ versus $1/T$, whose slope determines the singlet-triplet excitation energy $\Delta = 6.5$ meV. (b) Thermal dependence of the inverse reduced correlation length (in blue), ξ_0/ξ_{SP}, calculated for 1D SP structural fluctuations in function of the reduced temperature T/T_{SP}^{MF} [31]. The filled circles give ξ_0/ξ_{SP} measured in PF_6-H12 [12,34], where $T_{SP}^{MF} \approx 60$ K. The figure outlines the temperature ranges of dominant amplitude and soliton fluctuations. It gives also the thermal dependence of the inverse correlation length ξ_G^{-1} and ξ_S^{-1} in these regimes. The crossover between these two regimes occurs when $\xi_S \approx \xi_G$ for $T^* \approx 0.38\,T_{SP}^{MF}$.

peaks at 12.5 meV and 18 meV in Fig. 4. In addition, as we shall see at the end of Sec. III A below, our powder study allows us to probe the lattice quasielastic critical scattering response, which develops above T_{SP} at the location of the Q_{SP} superlattice reflection.

As the phonon contribution does not vary appreciably in temperature, and in order to probe quantitatively the thermal evolution of the magnetic excitation spectrum, which is responsible for the drop of intensity detected below 40 K in Fig. 4, we shall use in the following differences of responses

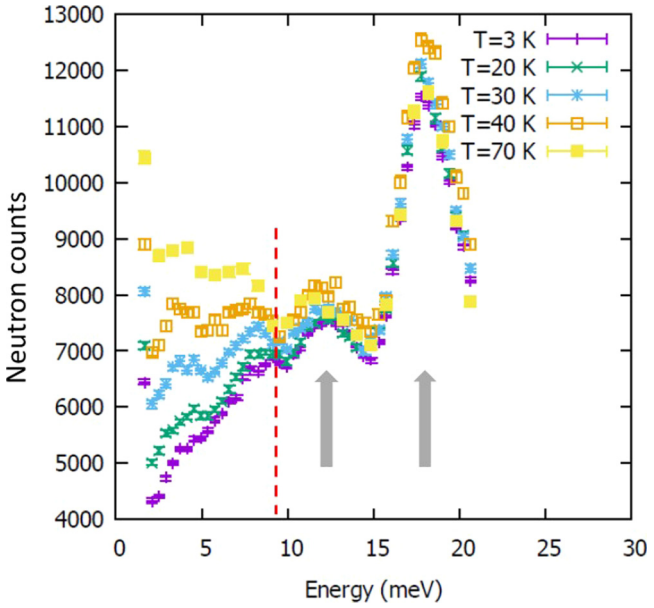

FIG. 4. Energy dependence of scattered neutron intensity measured in PF_6-D12 during run 1 at $Q = 1.66$ Å^{-1} for selected temperatures between 3 and 70 K. Note the large thermal dependence of the scattered intensity below ~9 meV. The gray arrows point towards two phonon branches at 12.5 meV and 18 meV. The background intensity is 2400.

$\Delta I(\omega, T) = I(Q_{SP}, \omega, T) - I(Q_{SP}, \omega, T_0)$ with respect to the response measured at a reference temperature T_0. Below we consider first $\Delta I(\omega,T)$ in the SP fluctuation regime between T_{SP}^{MF} and $T_{SP} = 13$ K, then second $\Delta I(\omega,T)$ in the SP ground state below T_{SP}.

A. Measurements above T_{SP}

The drop of intensity observed below 40 K in Fig. 4 can be precisely analyzed by the scan differences $\Delta I(\omega, T) = I(Q_{SP}, \omega, T) - I(Q_{SP}, \omega, 54\,\text{K})$; the reference of temperature, $T_0 = 54$ K, is taken in the middle of the temperature range 40–70 K, where $I(Q_{SP}, \omega, T)$ does not vary appreciably. Figure 5(a) shows the energy dependence of selected $\Delta I(\omega,T)$ differences for $T \leqslant 40$ K. At 30 K and below, when the energy decreases, the data exhibits, after a slight increase of intensity at high energy, a significant drop of intensity below 9 meV. As a consequence $\Delta I(\omega,T)$ exhibits a noticeable kink around ~9 meV. Below this last frequency, the amplitude of the intensity drop of $\Delta I(\omega,T)$ for T lower than 40 K is more precisely illustrated by Fig. 5(b), which reports the intensity difference A_{PG} of $\Delta I(\omega,T)$ between about 9 meV and 5 meV [see inset of Fig. 5(b)]. In Sec. IV A, we shall interpret the intensity drop of $\Delta I(\omega,T)$ by the formation of a pseudogap in the spin excitation spectrum below 9 meV.

Well inside the pseudogap structure, Fig. 5(a) shows that a new response emerges for energies lower than 6/4 meV at 30/13 K. Between these two last temperatures, the intensity of this response increases by a factor 2.5 at 1.7 meV. This is accompanied by a sharpening of the low energy response upon cooling. Both features reveal the growth of a critical quasielastic response. Such a response can be approximately

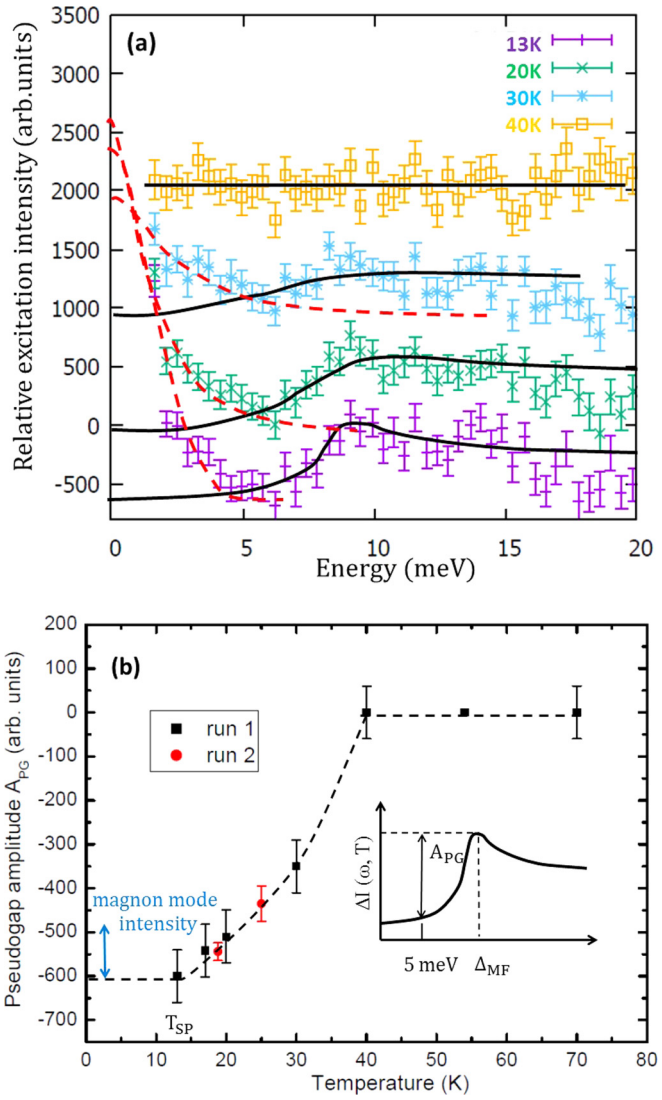

FIG. 5. (a) Energy scan differences issued from run 1, $\Delta I(\omega,T) = I(Q_{SP}, \omega, T) - I(Q_{SP}, \omega, 54\,K)$ for $T = 40$, 30, 20, and 13 K. At each T the continuous black line is an adjustment of the energy dependence of the data above 5 meV by that of the pseudogap density of states due to 1D Peierls fluctuations calculated in the LRA theory for the same T/T_P^{MF} ratio (T_P^{MF} being taken at 40 K). The quasielastic response observed below 5 meV has been adjusted to a Lorentzian at 30 K and 20 K and to a Gaussian at 13 K (dashed red lines). Data obtained at different T have been shifted. (b) Thermal dependence of the amplitude of the pseudogap A_{PG} obtained from the difference of $\Delta I(\omega,T)$ between its minimum (∼5 meV) and its maximum ($\Delta_{MF} \approx 9$meV) intensities in the scans shown in part (a). The relative intensity of the magnon mode detected below T_{SP} (Fig. 6) is also indicated.

fitted with a Lorentzian profile at 30 K and 20 K and more likely with a resolution-limited (1.7 meV, HWHM) Gaussian profile at 13 K (= T_{SP}). This quasielastic critical response will be analyzed in Sec. IV B.

B. Measurements below T_{SP}

Figure 6 reports the differences $\Delta I(\omega, T) = I(Q_{SP}, \omega, T) - I(Q_{SP}, \omega, 13\,K)$ between data measured in the SP

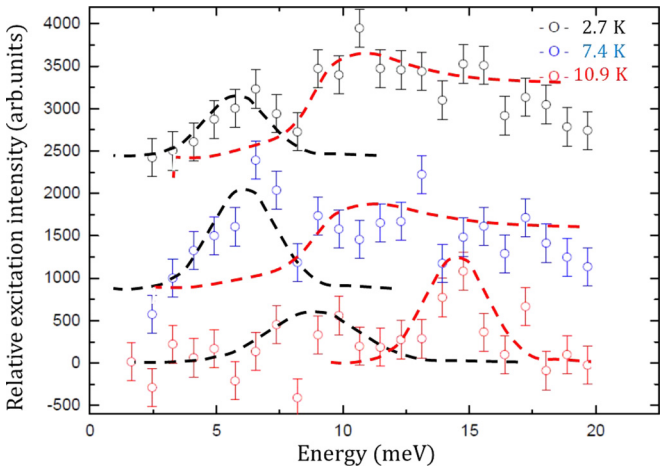

FIG. 6. Energy scan differences issued from run 2, $\Delta I(\omega, T) = I(Q_{SP}, \omega, T) - I(Q_{SP}, \omega, 13\,K)$ at $T = 10.9$, 7.4, and 2.7 K and its decomposition into low energy (dashed black lines) and high energy (dashed red lines) responses. The low energy responses and the high energy response at 10.9 K have been fitted by Gaussian, and the high energy responses at 2.7 and 7.4 K have been adjusted by an asymmetric profile similar to the ones used for the fit of the continuum excitation spectrum of Fig. 4(a). The intensity of these excitations represents ∼20% of the amplitude of the pseudogap at 13 K [Fig. 5(b)]. Data obtained at different T have been shifted.

ground state with respect to the pseudogap structure established at $T_{SP} = 13$ K (= T_0). Data at 2.7 K and 7.4 K are taken well inside the SP ground state. Data taken at 10.9 K are close to T_{SP}. First, $\Delta I(\omega,T)$ is positive for $T < T_{SP}$, which means that the decrease of neutron scattered intensity below 9 meV due to the progressive formation of a pseudogap below 40 K has stopped at T_{SP}. Second, Fig. 6 shows the growth below T_{SP} of a two peak structure corresponding to the establishment of two new excitations in the SP ground state.

The peak of lowest energy corresponds to a well-defined excitation that can be fitted by a Gaussian centered at 6.3_5, 6.4, and ∼9 meV at 2.7, 7.4, and 10.9 K, respectively. The energy of this excitation increases in the vicinity of T_{SP}. In addition, while the peak has about the experimental resolution in energy at 2.7 K and 7.4 K (1.5 meV HWHM), it significantly broadens by about 50% at 10.9 K (2.2 meV HWHM).

The high energy excitation has an asymmetric profile resembling that of the pseudogap structure observed above T_{SP} [see Fig. 5(a)]. This excitation shifts towards higher energy upon heating with a broad maximum of intensity located around 11, 11.5, and 15 meV at 2.7, 7.4, and 10.9 K, respectively.

These two excitations, which are also revealed by single crystal measurements performed at 1.4 K (see Appendix A) will be analyzed in Sec. IV C.

IV. ANALYSIS OF THE DATA

A. The pseudogap structure above T_{SP}

Theory predicts that in the adiabatic limit [21,30], SP structural fluctuations trigger the growth of a pseudogap in the continuum of AF magnetic excitations below an energy scale Δ_{MF} [Fig. 2(a)]. The Δ_{MF} can be estimated

at 9 meV from the observation of a net kink in the energy dependence of $\Delta I(\omega,T)$ [see Fig. 5(a)]. Figure 5(b) gives the thermal evolution of the amplitude of the pseudogap, A_{PG}, which develops below Δ_{MF} by plotting as a function of the temperature the difference of $\Delta I(\omega,T)$ between its minimum ($\sim$5m eV) and maximum (Δ_{MF}) intensities. It clearly shows that A_{PG} develops below 40 K.

It is interesting to remark that the characteristic energy scale $\Delta_{MF} \approx 9\,\text{meV}$ leads to $T_{SP}^{MF} \approx 40\,\text{K}$ via the mean-field relationship $\Delta^{MF} \approx 2.47\, k_B T_{SP}^{MF}$ obtained in the adiabatic theory [22]. Consistently, $T_{SP}^{MF} \approx 40\,\text{K}$ corresponds to the temperature below which the pseudogap rapidly develops [see Fig. 5(b)].

The role of fluctuations in the development of a pseudogap in the density of states of magnetic excitations can be clearly assessed by remarking that at a given reduced temperature T/T_{SP}^{MF}, the frequency dependence of $\Delta I(\omega,T)$ follows quite well the reduced density of states $D(\omega,T)/D_0$ of the fluctuating Peierls chain [see Fig. 5(a)], such as the one calculated by the Lee Rice Anderson (LRA) theory [30] for the same T/T_P^{MF} reduced temperature. In the LRA theory, $D(\omega,T)$ is the energy dependent electronic density of states in the presence of $2k_F$ Peierls fluctuation, and D_0 is the bare density of states at the Fermi level, $\omega = 0$, in absence of fluctuations. Note that the analogy between the density of states of magnetic excitations and the one electron density of states of the Peierls chain is justified for the XY SP system, which is described by the same Hamiltonian as one of the half-filled Peierls chain [16]. For a weakly localized SP chain under the influence of AF quantum fluctuations, relevant for the Fabre salts, the expression of the magnetic response $I_{mag.}(q_{SP},\,\omega,\,T)$ is a little more elaborated. The magnetic response at the wave vector $2k_F(=q_{SP})$ and frequency ω is proportional to the imaginary part of the dynamic spin susceptibility $\chi''(2k_F,\omega,T)$, which is calculated in Ref. [31] and recalled in Appendix B by expression (B1). It reads for temperature below T_{SP}^{MF},

$$I_{mag.}(q_{SP},\,\omega,\,T) \propto D(\omega,T)/D_0\,[\max(\omega,T)/T_\rho]^{-\gamma^*}. \quad (3)$$

The second member of expression (3) is the product of the density of states $D(\omega,T)/D_0$ (normalized by the bare limit D_0) in the presence of SP lattice fluctuations, namely the pseudogap effect, times the power law of the AF response function. The AF power law is controlled by the relative amplitude of the frequency ω and temperature T, with a critical exponent γ^*, which is itself reduced from unity by the pseudogap factor $D(\omega,T)/D_0$ in the density of states.

Thus when T decreases below the frequency scale ω, the power law enhancement of AF correlations levels off. Their amplitude is reduced for $\omega \leqslant \Delta_{MF}$ by the pseudogap factor $D(\omega,T)/D_0$. The AF correlations are also reduced, though to a lesser degree, through the exponent γ^*, which decreases below unity by the same density of states factor $D(\omega,T)/D_0$ for $\omega < \Delta_{MF}$ and $T < T_{SP}^{MF}$.

These properties of the magnetic response function capture fairly well the results of Fig. 5. Below 40 K for instance, the lowering of scattered intensity is clearly perceptible for $\omega \sim 5\,\text{meV}$, which is smaller than the scale Δ_{MF} but higher than the temperature. The reduction of scattering intensity in this frequency range, as shown in Fig. 5(b), is therefore dominated by the reduction of the density of states factor in expression (3) in the pseudogap regime. By contrast, and according to expression (3), the scattering intensity should start to increase again at lower frequency, namely when $\omega < T$. Such an increase results from the restoration of the power law enhancement of AF correlations, with a reduced, but still positive γ^*, which compensates the decay in the density of states as the temperature is lowered. The low frequency increase of the scattered intensity merges with the growing of a quasielastic component (see Sec. IV B below). It is noteworthy that a low frequency increase of AF correlations, though attenuated by the SP pseudogap, is also found from the low energy ^{13}C nuclear magnetic resonance (NMR) probe for spin-lattice relaxation rate of PF_6-H12 below 40 K [32].

Figure 5 shows that frequency and thermal evolutions of the pseudogap is slightly more marked for the SP chain than for the Peierls chain, especially when T_{SP}^{MF} is approached. In particular, Fig. 5(a) shows that the kink around $\Delta_{MF} \approx 9\,\text{meV}$ in the frequency dependence of $\Delta I(\omega,T)$ remains marked at 20 K and 30 K, while $D(\omega,T)/D_0$ given by the LRA theory exhibits a smoother energy variation at these temperatures [30]. Such a kink, followed by a smooth decrease of $\Delta I(\omega,T)$ for $\omega \geqslant \Delta_{MF}$, could be explained by the frequency dependence of the AF response function. Note, however, that the frequency dependence of the data above Δ_{MF} should be more attenuated than expected because Fig. 5(a) does not plot $I(q_{SP},\,\omega,\,T)$ itself, but the difference $\Delta I(\omega,\,T) = I(Q_{SP},\,\omega,\,T) - I(Q_{SP},\,\omega,\,54\,\text{K})$ with respect to 54 K.

By the formation of a well-pronounced pseudogap below $T_{SP}^{MF} \approx 40\,\text{K}$ [Fig. 5(b)], well above T_{SP}, our paper shows that the SP transition of PF_6-D12 occurs in the adiabatic limit. This finding should be contrasted with a previous inelastic neutron scattering investigation of the inorganic SP compound $CuGeO_3$, located in the antiadiabatic region, which does not reveal the growth of a pseudogap in the excitation pattern above T_{SP} [33].

B. The SP fluctuations above T_{SP}

The regime of adiabatic SP fluctuations in the Fabre salts has been quantitatively analyzed using the theoretical treatment of the SP chain in the weakly localized limit [31]. Figure 3 reports the calculated thermal dependence of (a) the spin susceptibility χ_S and of (b) the inverse SP structural correlation length, ξ_{SP}^{-1} in the 1D regime of SP fluctuations. In (a), the calculated χ_S, which has been adjusted to the experimental data of PF_6-D12 with $T_{SP}^{MF} \approx 40\,\text{K}$, decreases more rapidly than experimental findings between T_{SP} and $2T_{SP}$. In (b), the calculated thermal dependence of the correlation length ratio ξ_0/ξ_{SP} is well followed by the PF_6-H12 experimental data previously obtained [12,34]. Fluctuations are dominated at high temperature by those of the amplitude of the SP order parameter and at low temperature, when a sizeable SP order is achieved for large ξ_{SP}, by the thermal excitation of SP pairing defects consisting in the formation of local solitons. The crossover between these two fluctuations regimes occurs around $T^* \approx 0.38 T_{SP}^{MF}$. Interestingly, T^* amounts to $\sim$15 K in PF_6-D12, temperature below which the longitudinal sound velocity critically drops [29]. Figure 5(b) shows that the SP pseudogap sizably develops in the regime of amplitude

fluctuations. However, Fig. 3(a) shows that χ_S decreases slowly in this regime and then decreases rapidly below $\sim T^*$ in the presence of soliton excitations. In the 1D soliton regime, Δ_{MF} represents the energy required to break paired spins. By this process, a spin singlet is dissociated into an uncoupled pair of soliton (S) antisoliton ($\bar{S}$) excitations in which each component, carrying a spin $\frac{1}{2}$, can propagate freely (this is true when SP chains are not 3D coupled) and thus contributes to the spin susceptibility χ_S. This free propagation gives rise to a continuum of excitations for energy higher than $\sim\Delta_{MF}$ [see Fig. 1(a)]. The net decrease of χ_S below T^* can be viewed as due to the large reduction of the number of solitons thermally excited upon cooling.

Let us now consider the role of lattice degrees of freedom in the SP instability mechanism. The spin-phonon interaction couples magnetic (pseudogap formation and thermal dependence of the spin susceptibility) and lattice (1D correlation length) quantities. Their thermal dependences are consistent with a SP instability occurring in the adiabatic limit. In this limit and in the mean-field approximation, it is generally expected [35] that the SP structural instability should be driven by the softening of a phonon mode at Q_{SP}. Our phonon measurements reported in Appendix A do not provide any evidence for the frequency softening of a peculiar Q_{SP} low frequency acoustic mode. On the contrary, these measurements provide evidence of a slight frequency hardening for the TA mode of lowest energy when T_{SP} is approached. In addition, the low energy data of Fig. 5(a) provide evidence for the development of a critical quasielastic scattering between T_{SP}^{MF} and T_{SP}. This critical scattering occurs at the position of the Q_{SP} superlattice reflection whose intensity sizably develops below T_{SP} [11,25]. It is thus tempting to attribute a structural origin to this critical scattering. Furthermore the Lorentzian shape of the scattering suggests that the quasielastic scattering is due to a lifetime effect of SP clusters. Deconvolution of profile by the experimental resolution leads to a damping of $\Gamma = 1.4 \pm 0.2$ meV (HWHM of the intrinsic Lorentzian) at 30 K. At this Γ corresponds a SP pair lifetime $\tau = h/\Gamma$ of 6×10^{-12} s. The Γ cannot be precisely determined at 20 K because the Lorentzian width is too close to the experimental resolution (within experimental errors, one estimates $\Gamma \leqslant 0.6$ meV). Thus below 20 K, τ should be significantly enhanced so that the SP lattice dynamics should be quite slow. This agrees with the observation of a divergent T_1^{-1} relaxation rate at ^{75}As NMR frequency below 20 K in $(TMTTF)_2AsF_6$ [36]. If one assumes a classical critical scattering regime, where the damping Γ linearly vanishes when T_{SP} is approached, namely,

$$\Gamma = \Gamma_{SP}\left|\frac{T_{SP} - T}{T_{SP}}\right|, \tag{4}$$

one gets a characteristic SP damping $\Gamma_{SP} \approx 1$ meV, at which corresponds the characteristic SP time $\tau_{SP} = h/\Gamma_{SP}$ of 4×10^{-12} s.

Since the typical size of SP pairs is $\xi_0 \approx 12$ Å near T_{SP}^{MF} [see Fig. 3(b) and Ref. [34]), while their time life is $\tau_{SP} \approx 4 \times 10^{-12}$ s, it follows that SP fluctuations have a characteristic velocity of $v_{SP} = \xi_0/\tau_{SP} \approx 300$ m/s. Given that v_{SP} amounts to a typical longitudinal sound velocity (300 m/s) in organics, as typically measured in TTF-TCNQ [37] or $(TMTSF)_2PF_6$ [38], the SP fluctuations should be controlled by acoustic modes.

Using these findings, the dynamics of the SP transition can be more deeply analyzed. Assuming that the transverse acoustic (TA) mode of frequency $\hbar\Omega_C \approx 3.6$ meV determined in Appendix A is involved in the SP instability, one gets for PF_6-D_{12}, $\Omega_C\tau_{SP} \approx 3.6$. In the mean field approximation, the crossover from displacive dynamics (i.e., with a critical phonon frequency softening) to order-disorder dynamics (i.e., with a critical damping) occurs for $\Omega_C \sim 1/\tau_{SP}$ [39]. This simple criteria places PF_6-D_{12} in the order-disorder limit. In this limit, the damping is due to the slowing down of the SP cluster life time τ, while the critical phonon frequency does not appreciably vary. Furthermore the observation of the critical growth of a central peak in energy in the neutron scattering spectrum [Fig. 5(a)], associated to a critical slowing down of the SP dynamics together with a slight frequency hardening of the TA mode (see Appendix A) means that the SP transition of the $(TMMTF)_2PF_6$ actually exhibits an order-disorder character [19,40]. Finally, the occurrence of a slow SP critical lattice dynamics is assessed by the detection in $(TMTTF)_2AsF_6$ of a divergent ^{75}As NMR T_1^{-1} relaxation rate [36]. Note that the NMR probe of ^{75}As critical T_1^{-1} in $(TMTTF)_2AsF_6$ shows that the critical dynamics should also involve the anion.

A previous investigation of $CuGeO_3$, revealing the critical growth of a central peak in energy [41] and the frequency hardening of the critical phonon mode [42], shows also that the SP critical dynamics of $CuGeO_3$ is of the order-disorder type [19]. Note, however, that a different dynamics of the displacive type, which consists in a critical phonon frequency softening, as predicted in Ref. [35], is observed in the SP parented compound TiOCl [43].

C. Excitations in the SP ground state

The scan difference $\Delta I(\omega, T)$ shown in Fig. 6 exhibits a double peak structure in the SP ground state, which superimposes to the pseudogap already established at T_{SP}. Thus below T_{SP}, two new excitations appear in the SP ground state. This means that the magnetic excitation spectrum of the SP chain changes in the SP ground state when the chain dimerization is 3D long-range ordered. In this respect, the SP transition should differ from the Peierls transition in which the 3D coupling simply transforms the pseudogap into a true gap in the electronic excitation processes.

The peak at lowest energy observed in Fig. 6, centered at 6.3_5 meV and 6.4 meV at 2.7 K and 7.4 K, respectively, corresponds to a well-defined excitation whose energy is congruent with the activation energy, $\Delta \approx 6.5$ meV, measured in the thermal dependence of the spin susceptibility χ_S below T_{SP} [see inset of Fig. 3(a)]. Note that Δ is the true gap of the SP transition, which, in contrast to the Peierls situation, remains distinct from the pseudogap scale Δ_{MF} as we enter in the ordered state. The gap Δ corresponds to the singlet-triplet excitation energy of the dimer. The propagation of this excitation in chain direction gives rise to the $S = 1$ magnon branch shown in Fig. 2(b) [44]. The low energy maxima of intensity in the powder spectra corresponds to the minimum energy of this branch at Δ. Note that the maximum of energy

of the magnon branch leads also to a maxima of intensity at $J_{\rm eff}$ in the powder diffraction spectra, which was been previously detected [24].

The minimum energy of the magnon branch, Δ, increases upon heating towards $T_{\rm SP}$, reaching a value $\sim$9 meV, close to $\Delta_{\rm MF}$, at 10.9 K. At this last temperature, the width of the magnon peak has significantly increased. At the extra broadening, a damping of $\Gamma_{\rm mag} \approx 1.1$ meV (HWHM of the intrinsic peak) corresponds. The $\Gamma_{\rm mag}$ corresponds to a short lifetime of the magnon, which can be estimated at $\tau_{\rm mag} \approx 4 \times 10^{-12}$ s. This lifetime effect could be due to the decay of the $S = 1$ magnon into two $S = 1/2$ solitons [see lower part of Fig. 2(a)] when, in the vicinity of $T_{\rm SP}$ sizable fluctuations, overcome the 3D interchain coupling (a relevant 3D coupling prevents the formation of solitons well below $T_{\rm SP}$). Note that the increase of χ_S at 10.9 K evidences the presence of sizable magnetic fluctuations [see the inset of Fig. 1 and Fig. 3(a)]. By the enhancement of such fluctuations, one expects a continuous merging at $T_{\rm SP}$ of the magnon mode into the pseudogap structure occurring in the continuum of spinon (soliton) excitations.

The high energy excitation peak revealed in Fig. 6 shows the occurrence of a very broad response. Furthermore, its asymmetric profile can be well adjusted (for the two lowest temperatures) by a pseudogap structure similar to the one used to analyze the magnetic response above $T_{\rm SP}$. Such a profile in the powder neutron scattering spectrum likely corresponds to a density of states of magnetic excitations. It proves the existence of a high energy continuum of quasi-1D magnetic excitations exhibiting a broad maxima in the density of states around 11, 11.5, and 15 meV ($\Delta_{\rm cont.}$) at 2.7, 7.4, and 10.9 K, respectively. According to the RPA theory of magnetic excitations in coupled dimerized AF chains [44], the high energy response observed in Fig. 6 should correspond to the low energy part of a continuum of free excitations of two magnons [see Fig. 2(b)]. According to this theory, the two-magnon excitation spectrum should start at 2Δ, in which the value is close to $\Delta_{\rm cont.}$ measured at 2.7 and 7.4 K.

A double gap excitation spectrum at Δ and 2Δ has been previously observed in the SP phase of $CuGeO_3$ [45]. However, the data of PF_6-D12 show that the SP excitation spectrum should progressively emerge below $T_{\rm SP}$ from the quasi-1D pseudogap structure established between $T_{\rm SP}^{\rm MF}$ and $T_{\rm SP}$. In this scenario, the well-defined magnon branch and the two magnon continuum of the SP phase should arise from a restructuration of the energy dispersion of the 1D pseudogap structure by the 3D interchain SP coupling. Our data show also that on approaching $T_{\rm SP}$ from below the one magnon excitation probably decays into two solitons. By this process, the continuum of two magnon excitations should progressively transform into a continuum of soliton (spinon) excitations upon heating. Since the interchain dimerization coupling energy is quite weak in the Fabre salts, as assessed by the detection of SP reflections of small intensity [11,25], this transformation should be progressive. This progressive transformation is also consistent with the detection of a weak SP excitation spectrum in Fig. 6 whose intensity amounts to about 20% of the reduction of scattered intensity due to the formation of the 1D pseudogap. To our knowledge, the transformation of the magnetic excitation spectrum across the critical temperature of a strongly anisotropic, quasi-1D SP system has not yet been considered in the literature.

V. GENERAL DISCUSSION

A. The magnetostructural coupling

Both magnetic and structural degrees of freedom exhibit sizable fluctuations on a large temperature range in the vicinity of $T_{\rm SP}$. The inset of Fig. 1 shows that $d\chi_S/dT$ varies sizably between 6 and 20 K, which represents a temperature range comparable to $T_{\rm SP}$ itself. Also, low frequency critical fluctuations probed by sound velocity [29], thermal lattice expansion [46], and anion NMR spin lattice relaxation [36] measurements extend on a similar temperature range. All these features are the signature of an important magnetoelastic coupling.

The strongest thermal expansion divergence at the SP transition is observed along the transverse c^* direction [9]. This finding confirms our suggestion that the critical phonon mode for the SP transition should be the lowest energy TA phonon mode polarized in the vicinity of the interlayer c^* direction, as revealed by single crystal measurements of Appendix A. Note that this critical TA phonon mode should displace both the TMTTF and the anion entities, as assessed by various NMR measurements [32,36]. The transverse polarization of this acoustic mode at $Q_{\rm SP}$ should involve general displacements, u_i, which modulate the short contact distance between TMTTF and PF_6 species. As each TMTTF molecule has an asymmetric anion environment (see Fig. 7), the $\pm u_D$ shift of the donor should modulate in a nonequivalent manner the hole distribution (i.e., spin $\frac{1}{2}$ location) within each TMTTF dimer. This, as well as the $\pm u_A$ anion shift, more explicitly considered in Fig. 7, modulate, to first order in lattice displacement u_i, the various intrastack electronic interactions such as the AF exchange interaction J. Such a lattice modulation, which changes charge/spin distribution in each dimer, should lead to an efficient first order magnetostructural coupling on each TMTTF stack of AF coupled spins 1/2. In particular, the anion shift toward the TMTTF, which attracts the hole, should be correlated with spin 1/2 (linked to the hole) displacement

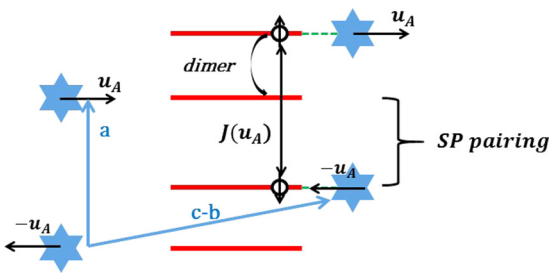

FIG. 7. Schematic representation of a TMTTF stack and its surrounding anion (blue stars). The initial charge/spin distribution shown is that of the CO phase with interdimer AF magnetic correlations. This figure illustrates the charge/spin transfer induced in the upper dimer by the anion displacements $+u_A$. Note that the anion displacements $-u_A$ stabilize the initial charge disproportion in the lower dimer. Such correlated lattice/charge displacements drive the singlet SP pairing. The relative anion displacements $\pm u_A$ are those of the TA mode of wave vector $(1/2, \frac{1}{2}, \frac{1}{2})$.

inside each dimer [47]. Correlated anion displacements should induce the pairing between neighboring spins into a singlet ground state (see Fig. 7). In this picture, anion displacement should also control the dynamics of SP pairing. As anions are certainly linked by H bonds to the outer methyl groups of TMTTF, delimiting its cavity, at T_{SP}^{MF} and below, as found in $(TMTSF)_2PF_6$ [48], such dynamics could be particularly slow. Thus anions could impose a relaxation or order-disorder dynamics exhibiting the critical slowing down observed at the SP transition. Note also that a critical slowing down associated to a relaxation dynamics was also observed at the CO/ferroelectric transition of AsF_6 [49] and PF_6-D12 [23] Fabre salts.

In this mechanism, illustrated by Fig. 7, it is interesting to remark that the SP instability in the weakly localized limit, relevant for the Fabre salts, should be also correlated to charge displacement on donor stacks. The relevance of such charge effects has been revealed by microwave dielectric constant measurements, which exhibit an anomaly at the SP transition of PF_6-D12 [23]. Interestingly, such dielectric measurements give a charge relaxation time of $\tau_{diel} \approx 4 \times 10^{-13}$ s above T_{SP} close to the SP life time τ_{SP}. This suggests, as expected, that charge and spin effects are intimately coupled in the SP instability mechanism of weakly localized systems.

B. The generic phase diagram of the Fabre salts

Let us now come back to the generic phase diagram of the Fabre and Bechgaard salts. Our data clearly show, by the formation of a sizeable pseudogap, that at ambient pressure the SP transition of PF_6-D12 occurs in the adiabatic limit. However, with a half mean field gap energy $\Delta_{MF}/2 \approx 4.5$ meV, only slightly larger than the TA critical phonon frequency $\hbar\Omega_C \sim 3.6$ meV, the SP transition should occur in the vicinity of the classical-quantum crossover [17].

For a weakly localized electron gas, it can be shown [see expression (C3) in Appendix C] that T_{SP}^{MF} is proportional to the charge localization temperature T_ρ. As in PF_6-H_{12}, T_ρ decreases by a factor 2.5 under a pressure of 9 kbar [5]; therefore, it is expected that T_{SP}^{MF} and Δ_{MF} should similarly diminish. The sizable decrease of Δ_{MF} should first drive for weak pressure $(TMTTF)_2PF_6$ into the antiadiabatic SP gapped phase. Second, at a larger pressure, one estimates with the same rate of decrease as T_ρ that Δ_{MF} should reach a value of ~3.6 meV around 9 kbar, comparable to the frequency of the critical TA mode at ambient pressure. Note that since the TA mode should harden under pressure, one estimates, using the rate of increase of the longitudinal acoustic (LA) phonon frequency of TTF-TCNQ upon cooling [50] for the same amount of parameter contraction, that under pressure the SP critical TA phonon frequency should increase by 22% under 9 kbar, reaching $\hbar\Omega_C \approx 4.4$ meV. Thus, one obtains at 9 kbar a ratio $\Delta_{MF}/\hbar\Omega_C \approx 0.8$ close to the range 0.6–0.8 of $\Delta_{MF}/\hbar\Omega_C$ critical ratios for which the SP ground state is suppressed by zero point phonon quantum fluctuations [18]. This quantitatively accounts for the observation of a QCP at $P_{QCP} \approx 9$ kbar in pressurized PF_6-H12 [6]. In this salt, when P tends to P_{QCP}, quantum fluctuations drive a singular drop of T_{SP}, while at P_{QCP} the stabilization of a spin liquid state exhibiting low D AF quantum fluctuations [6]. However when P moves away from P_{QCP}, the increase of the interchain magnetic coupling drives the spin quantum system to a 3D AF ground state, whose critical temperature T_{AF} singularly increases under pressure.

Finally, we want to point out that the SP instability is controlled by two distinct criteria of adiabaticity. The first one, which compares $\hbar\Omega_C$ with $\Delta_{MF}/2$, controls the classical or quantum nature of the SP ground state. The second one, which compares Ω_C with $1/\tau_{SP}$, controls the displacive or order-disorder character of the critical dynamics of the SP transition. Our ambient pressure study of the Fabre salts shows, using these two criteria of adiabaticity, that a classical SP ground state can exhibit an order-disorder critical dynamic. It has been recently pointed out that these two adiabaticity criteria are also relevant for the Peierls instability [39,51].

VI. CONCLUSION

In conclusion, we have performed the first inelastic neutron scattering study of SP magnetic excitations induced by a strong magnetoelastic coupling with low frequency lattice degrees of freedom in an organic material. Due to this coupling, our paper reveals the presence of sizable critical fluctuations developing on a large temperature range on each side of T_{SP}. More precisely, our data reveal the formation of a pseudogap in the AF magnetic excitation spectrum concomitant with the growth of 1D SP structural fluctuations associated to an order-disorder or relaxation dynamics. Below T_{SP}, the 3D interchain coupling leads to the emergence of a two gapped magnetic excitation spectrum in the high temperature 1D pseudogap structure. These features show that Fabre salts are located at ambient pressure in the adiabatic/classical gapped limit of the SP phase diagram. An estimation of the pressure dependence of microscopic parameters controlling the SP instability shows that pressurized Fabre salts should easily move to the antiadiabatic/quantum SP gapped phase, which ends to a QCP when the competition between AF and zero point quantum fluctuations prevails. Our paper shows that an accurate interpretation of the generic phase diagram of the Fabre and Bechgaard salts cannot ignore the coupling between electronic/spin and structural degrees of freedom.

APPENDIX A: THE Q_{SP} ENERGY SCAN IN A PF_6-D_{12} SINGLE CRYSTAL

Figure 8 represents two energy scans at the Q_{SP} reciprocal position in the $[a^*, b^* - c^*]$ reciprocal plane of a single crystal of PF_6-D_{12} at temperatures above and below T_{SP}.

Data taken above T_{SP} at the reduced Brillouin zone corner $(1/2, \frac{1}{2}, \frac{1}{2})$ reveal three phonons modes at $3.5_6/4.1/4.1$ meV, $8.1/8.3/7.9$ meV, and 11.1_5 meV at 20/17/15.8 K, respectively. The lower two frequencies are close to the frequencies of the TA mode polarized along the short molecular axis (4.5 meV) and of the LA mode (7.2 meV) measured at a similar reduced wave vector $(b^*/4)$ in TTF-TCNQ at room temperature (RT) [52] [in stack direction $b^*/4$ in TTF-TCNQ corresponds to $a^*/2$ in $(TMTTF)_2PF_6$]. Note that in TTF-TCNQ, the other TA mode (5 meV) polarized along the long molecular axis bears the $2k_F$ Kohn anomaly at the origin of its Peierls transition [53].

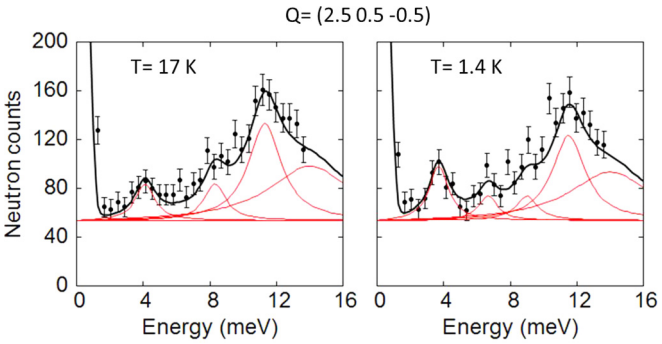

FIG. 8. Energy scans at $Q_{SP} = (2.5, 0.5, -0.5)$ at 17 K (left side) and 1.4 K (right side) in a single crystal of PF_6-D12. The fit of the scan at 17 K reveals the presence of three phonons modes at 4.11 ± 0.25, 8.27 ± 0.25, and 11.16 ± 0.20 meV plus an additional response at larger energy. The fit of the scan at 1.4 K reveals, in addition to three phonon modes at 3.67 ± 0.13, 8.81 ± 0.27, and 11.16 ± 0.20 meV, an additional response at 6.66 ± 0.25 meV.

The inelastic neutron scattering investigation in the SP phase at 1.4 K reveals, in addition to the three phonon modes at $3.7/8.8/11.1_5$ meV, an additional excitation at 6.66 ± 0.25 meV. The energy of this last excitation corresponds to the low energy excitation found at 6.4 meV in the powder spectrum of Fig. 6. This energy corresponds to the energy gap of the magnon branch Δ [Fig. 2(b)] or to the singlet–triplet excitation energy of χ_S [Fig. 3(a)]. Also, the difference between spectra recorded at 1.5 K and 20 K (not shown here) provides evidence of an asymmetric broad excitation with a large maxima in energy around 12.5 meV, resembling the high energy excitation revealed in Fig. 6.

The lowest frequency phonon mode probably corresponds to a TA mode polarized along the $b^* - c^*$ direction, which is close to the short molecular axis. This phonon mode exhibits an anomalous thermal dependence since its frequency hardens by 14% when the temperature approaches T_{SP} (from 3.5_6 meV at 20 K to 4.1 meV at 15.8 K), then softens back to 3.7 meV at 1.4 K in the SP phase. Such an antisoftening effect at T_{SP} is expected for the critical SP dynamics in the order-disorder limit [19,40].

APPENDIX B: EXPRESSION OF THE 1D MAGNETIC RESPONSE IN PRESENCE OF SP LATTICE FLUCTUATIONS IN THE WEAKLY LOCALIZED LIMIT

The magnetic response at the wave vector $2k_F(=q_{SP})$ is proportional to the imaginary part of the dynamic spin susceptibility $\chi''(2k_F,\omega,T)$ at $2k_F$ and frequency ω. In the framework of the renormalization group method for a 1D electron system in interaction at half filling [31], the two-loop expression of the dynamic spin susceptibility $\chi(2k_F,\omega,T)$, with a Hartree coupling of electrons to SP degrees of freedom below T_{SP}^{MF} (derived in Appendix C) is given by

$$\chi''(2k_F,\omega,T) = D(\omega,T)\left(\frac{\max(\omega,T)}{T_{SP}^{MF}}\right)^{-\gamma*(T)} [1 - 2n_F(\omega/2)] \tag{B1}$$

where n_F is the Fermi distribution factor. Here $D(\omega,T)$ is the density of states renormalized by SP lattice fluctuations in the LRA approximation [30]. The power law expression is proportional to the real part of the dynamic spin susceptibility at $2k_F$ and $\gamma^*(T) = D(\omega,T)/D_0$ is the exponent of the susceptibility renormalized downward from unity by SP lattice fluctuations. Here D_0 is the bare density of state equal to the inverse of the longitudinal electron bandwidth.

APPENDIX C: THE T_{SP}^{MF} IN THE WEAK LOCALIZED LIMIT

In the adiabatic case where phonon degrees of freedom are considered as classical, the SP instability of the organic salt results from the coupling of bond-centered $2k_F$ CDW (bond order wave [BOW]) correlations to lattice degrees of freedom. Treated in the mean-field approximation [31], the coupling leads to the condition

$$1 - D_0\, g_{ph}\, \chi_{BOW}\left(2k_F, T_{SP}^{MF}\right) = 0. \tag{C1}$$

It defines the 1D mean-field scale of the SP instability T_{SP}^{MF}. In expression (C1), g_{ph} is proportional to the square of the electron-phonon coupling constant.

$$\chi_{BOW}\left(2k_F, T_{SP}^{MF}\right) = D_0\, C\left(\frac{T}{T_\rho}\right)^{-\gamma} \tag{C2}$$

is the $2k_F$ BOW susceptibility of the interacting electron gas. Below the Mott scale, T_ρ, the BOW susceptibility exhibits a power law singularity in temperature with $\gamma = 1$ at half filling. Here C (>1) is a constant that includes the influence of BOW fluctuations above T_ρ. The mean-field criteria (C1) then yields the expression for T_{SP}^{MF}:

$$T_{SP}^{MF} = C\, D_0 g_{ph} T_\rho. \tag{C3}$$

It fixes a scale for the onset of strong BOW correlations proportional to T_ρ. When the Mott scale T_ρ becomes large, namely of the order of the electron bandwidth, ${D_0}^{-1}$, expression (C3) becomes $T_{SP}^{MF} \sim g_{ph}$, corresponding to the strongly localized (Heisenberg) limit treated by Cross and Fischer [35].

[1] D. I. Komskii, *Basic Aspects of the Quantum Theory of Solids* (Cambridge University Press, Cambridge, UK, 2010).
[2] J. Orenstein and A. J. Millis, Science **288**, 468 (2000).
[3] K. Rossnagel, J. Phys.: Condens. Matter **23**, 213001 (2011).
[4] *Springer Series in Materials Sciences: The Physics of Organic Conductors and Superconductors*, edited by A. G. Lebed (Springer-Verlag, Berlin, 2008), Vol. 110.
[5] C. Bourbonnais and D. Jérome, in Ref. [4], p. 357.
[6] D. S. Show, P. Wzietek, D. Folliatti, B. Alavi, D. J. Tantillo, C. A. Merlic, and S. E. Brown, Phys. Rev. Lett. **81**, 3984 (1998).
[7] N. Doiron-Leyraud, P. Auban-Senzier, S. R. de Cotret, C. Bourbonnais, D. Jérome, K. Bechgaard, and L. Taillefer, Phys. Rev. B **80**, 214531 (2009).
[8] M. de Souza and J. P. Pouget, J. Phys.: Condens. Matter **25**, 343201 (2013).

[9] M. de Souza, P. Foury-Leylekian, A. Moradpour, J.-P. Pouget, and M. Lang, Phys. Rev. Lett. **101**, 216403 (2008).

[10] P. Foury-Leylekian, S. Petit, G. Andre, A. Moradpour, and J. P. Pouget, Physica B **405**, S95 (2010).

[11] P. Foury-Leylekian, D. Le Bolloc'h, B. Hennion, S. Ravy, A. Moradpour, and J.-P. Pouget, Phys. Rev. B **70**, 180405(R) (2004).

[12] J. P. Pouget, R. Moret, R. Comès, K. Bechgaard, J. M. Fabre, and L. Giral, Mol. Cryst. Liq. Cryst. **79**, 485 (1982).

[13] J. P. Pouget and S. Ravy, J. Phys. I (France) **6**, 1501 (1996).

[14] J. P. Pouget and S. Ravy, Synth. Metals **85**, 1523 (1997).

[15] H. Bakrim and C. Bourbonnais, Phys. Rev. B **90**, 125119 (2014).

[16] L. G. Caron and S. Moukouri, Phys. Rev. Lett. **76**, 4050 (1996).

[17] R. Citro, E. Orignac, and T. Giamarchi, Phys. Rev. B **72**, 024434 (2005).

[18] A. Weiße, G. Hager, A. R. Bishop, and H. Fehske, Phys. Rev. B **74**, 214426 (2006).

[19] J. P. Pouget, Eur. Phys. J. B **20**, 321 (2001); **24**, 415 (2001).

[20] J. P. Pouget, Physica B **407**, 1762 (2012).

[21] L. Dumoulin, C. Bourbonnais, S. Ravy, J. P. Pouget, and C. Coulon, Phys. Rev. Lett. **76**, 1360 (1996).

[22] E. Orignac and R. Chitra, Phys. Rev. B **70**, 214436 (2004).

[23] A. Langlois, M. Poirier, C. Bourbonnais, P. Foury-Leylekian, A. Moradpour, and J. P. Pouget, Phys. Rev. B **81**, 125101 (2010).

[24] P. Foury-Leylekian, S. Petit, C. Coulon, B. Hennion, A. Moradpour, and J.-P. Pouget, Physica B **404**, 537 (2009).

[25] J. P. Pouget, P. Foury-Leylekian, D. Le Bolloc'h, B. Hennion, S. Ravy, V. Cardoso, and A. Moradpour, J. Low Temp. Physics **142**, 147 (2006).

[26] P. Wzietek, F. Creuzet, C. Bourbonnais, D. Jérome, K. Bechgaard, and P. Batail, J. Phys. I (France) **3**, 171 (1993).

[27] S. Eggert, I. Affleck, and M. Takahashi, Phys. Rev. Lett. **73**, 332 (1994).

[28] B. Salameh, S. Yasin, M. Dumm, G. Untereiner, L. Montgomery, and M. Dressel, Phys. Rev. B **83**, 205126 (2011).

[29] M. Poirier, A. Langlois, C. Bourbonnais, P. Foury-Leylekian, A. Moradpour, and J. P. Pouget, Phys. Rev. B **86**, 085111 (2012).

[30] P. A Lee, T. M. Rice, and P. W. Anderson, Phys. Rev. Lett. **31**, 462 (1973).

[31] C. Bourbonnais and B. Dumoulin, J. Phys. I **6**, 1727 (1996).

[32] F. Creuzet, C. Bourbonnais, L. G. Caron, and K. Bechgaard, Synth. Metals, **19**, 289 (1987).

[33] L. P. Regnault, M. Ain, B. Hennion, G. Dhalenne, and A. Revcolevschi, Phys. Rev. B **53**, 5579 (1996).

[34] J. P. Pouget, Crystals **2**, 466 (2012).

[35] M. C. Cross and D. S. Fischer, Phys. Rev. B **19**, 402 (1979).

[36] F. Zamborszky, W. Yu, W. Raas, S. E. Brown, B. Alavi, C. A. Merlic, A. Baur, S. Lefebvre, and P. Wzietek, J. Phys. IV France **12**, 9 (2002).

[37] T. Tiedje, R. R. Haering, M. N. Jericho, W. A. Roger, and A. Simpson, Solid State Commun. **23**, 713 (1977).

[38] P. M. Chaikin, T. Tiedje, and A. N. Bloch, Solid State Commun. **41**, 739 (1982).

[39] J. P. Pouget, C. R. Phys. **17**, 332 (2016).

[40] C. Gros and R. Werner, Phys. Rev. B **58**, R14677 (1998).

[41] K. Hirota, G. Shirane, Q. J. Harris, Q. Feng, R. J. Birgeneau, M. Hase, and K. Uchinokura, Phys. Rev. B **52**, 15412 (1995).

[42] M. Braden, B. Hennion, W. Reichardt, G. Dhalenne, and A. Revcolevschi, Phys. Rev. Lett. **80**, 3634 (1998).

[43] E. T. Abel, K. Matan, F. C. Chou, E. D. Isaacs, D. E. Moncton, H. Sinn, A. Alatas, and Y. S. Lee, Phys. Rev. B **76**, 214304 (2007).

[44] G. S. Uhrig and H. J. Schulz, Phys. Rev. B **54**, R9624(R) (1996).

[45] M. Aïn, J. E. Lorenzo, L. P. Regnault, G. Dhalenne, A. Revcolevschi, B. Hennion, and Th. Jolicoeur, Phys. Rev. Lett. **78**, 1560 (1997).

[46] M. de Souza, A. Brühl, J. Müller, P. Foury-Leylekian, A. Moradpour, J.-P. Pouget, and M. Lang, Physica B **404**, 494 (2009).

[47] J. P. Pouget, Physica B **460**, 45 (2015).

[48] P. Foury-Leylekian, S. Petit, I. Mirebeau, G. André, M. de Souza, M. Lang, E. Ressouche, A. Moradpour, and J.-P. Pouget, Phys. Rev. B **88**, 024105 (2013).

[49] D. Starešinić, K. Biljaković, P. Lunkenheimer, and A. Loidl, Solid State Commun. **137**, 241 (2006).

[50] J. P. Pouget, S. M. Shapiro, G. Shirane, A. F. Garito, and A. J. Heeger, Phys. Rev. B **19**, 1792 (1979).

[51] Similarly, the two criteria of adiabaticity of the Peierls chain compare $\hbar\Omega_{2k_F}$ with the mean field Peierls gap $2\Delta_{\mathrm{MF}}$ (instead of Δ_{MF} indicated in Ref. [39]) and Ω_{2k_F} with the inverse life time of the electron-hole pair, $1/\tau_{\mathrm{eh}}$.

[52] R. Comès and G. Shirane, in *Highly Conducting One-Dimensional Solids*, edited by J. T. Devresse, R. P. Evrard, and V. E. van Doren (Plenum Press, New York, 1979), Chap. 2.

[53] G. Shirane, S. M. Shapiro, R. Comès, A. F. Garito, and A. J. Heeger, Phys. Rev. B **14**, 2325 (1976).